05.6

Effect of annealing in different medium on the properties of calcium fluoride nanopowder

© S.Yu. Sokovnin[1,2], V.G. Ilves[1], M.A. Uimin[2,3]

[1] Institute of Electrophysics, Ural Branch, Russian Academy of Sciences, Yekaterinburg, Russia
[2] Ural Federal University after the first President of Russia B.N. Yeltsin, Yekaterinburg, Russia
[3] M.N. Mikheev Institute of Metal Physics, Ural Branch, Russian Academy of Sciences, Yekaterinburg, Russia
E-mail: sokovnin@iep.uran.ru

Received April 28, 2022
Revised August 29, 2022
Accepted August 29, 2022

Using a pulsed electron beam evaporation in vacuum a mesoporous nanopowder CaF_2 with a specific surface area up to 60.5 m^2/g were produced. The effect of annealing in different media on the evolution of magnetic and texture properties of CaF_2 nanoparticles has been studied. For the first time, the effect of annealing medium on the specific surface area and magnetization of CaF_2 nanopowders was discovered.

Keywords: nanopowders, calcium fluoride, ferromagnetism, electron beam evaporation.

DOI: 10.21883/TPL.2022.10.54800.19240

Nanopowders (NPs) feature unique properties related to the size factor and other specifics of their internal structure (most notably, the structure imperfection and the composition and shape of nanoparticles). This is especially true for NPs synthesized using physical methods: laser evaporation [1] or plasma synthesis [2]. However, NPs produced by mechanical grinding from pure (and, in particular, doped) CaF_2 exhibit room-temperature ferromagnetism (RTFM) [3]. Out of all known methods of NP synthesis relying on the evaporation–condensation principle, pulsed electron beam evaporation (PEBE) in vacuum provides NPs with the highest number of defects of various types [4].

The advantages of PEBE in application to fluorides are as follows. Since synthesis proceeds in vacuum, the pyrohydrolysis reaction is excluded. Both nanosized coatings and powders of various compositions (from simple fluorides to complex ones) may be obtained. The method does not require hazardous fluoride-containing precursors. Lastly, it provides a production rate sufficient to synthesize such amounts of nanopowder that are needed to perform a complete set of physical and chemical studies [4]. The specific surface area (SSA) was 64.3 m^2/g in the as-synthesized NP and increased to 88.7 m^2/g [4] after heating to 200°C. The CaF_2 NP had a large interparticle pore volume, which increased after heating to 200°C (from 0.25 to 0.66 cm^3/g). The diameter of pores also increased from 21 to 29 nm in the process. The texture properties specified above make this NP a promising agent for targeted drug delivery.

The obtained BNP exhibited RTFM, which became more pronounced (went from 0.045 to 0.06 emu/g) after annealing at 200°C. Following annealing at 900°C, the NP returned to its initial diamagnetic state [5]. It was demonstrated in [5] that RTFM of CaF_2 nanoparticles is their intrinsic property and is not associated with foreign magnetic impurities (e.g., 3*d* metals). It was concluded that complex defects, which transform during annealing and induce a shift of red peaks in the pulse cathodoluminescence spectra toward longer wavelengths, are the likely causes of emergence of RTFM. Fluoride vacancies, impurity oxygen vacancies, and interstitial fluoride ions are most likely involved in the formation of magnetic defects. Notably, the results of joint thermal analysis (DSC-TG) verified the presence of metallic Ca nanoparticles in the CaF_2 NP synthesized in vacuum, and the formation of CaO nanoparticles in the process of annealing was confirmed by photoluminescence and pulse cathodoluminescence. The formation of CaO was also observed in plasma synthesis of CaF_2 [2].

The aim of the present study is to examine the variation of properties of CaF_2 NPs after annealing in different gaseous media (air, vacuum, argon).

Mesoporous nanocrystalline calcium fluoride powders were prepared by PEBE in vacuum [4]. The NP synthesis procedure was detailed in [5]. NPs were annealed in different gaseous media (air, vacuum, argon) in a PM-1400A muffle furnace with SiC heating elements, program control, and a temperature accuracy of ±1°C (type *S* platinum/platinum-rhodium couple). Using a vacuum pump, one could establish vacuum (5 kPa, YTN-60H pressure sensor, ±3%) inside the furnace and then inject the needed gas. The pressure during annealing in argon (99.998%, GOST 10157−79) was slightly higher than the atmospheric one (120 kPa). The heating rate was 20°C/min for all samples. Isothermal annealing was performed for 10 min, and then the samples were cooled at the same rate to room temperature together with the furnace. The NP samples before and after annealing at a temperature of 200, 400, and 900°C are hereinafter denoted as *S*0, *S*200, *S*400, and *S*900, respectively. Lower indices *Atm*, *Vac*, and

Table 1. Texture properties of CaF_2 NP

Sample	SSA, m^2/g			Interparticle pore volume, cm^3/g			Diameter, nm		
	Atm	*Vac*	Ar	*Atm*	*Vac*	Ar	*Atm*	*Vac*	Ar
*S*0		64.3			0.25			21	
*S*200	88.7	49.9	58.7	0.66	0.34	0.43	29	29	25.95
*S*400	52.4	46.1	40.1	0.30	0.37	0.42	22.5	33.4	26.62
*S*900	1.11	0.15	2.39	0.0025	–	0.0031	37	–	18.73

Table 2. Relative crystalline phase content and mean size of the coherent scattering region (CSR)

Sample	CaF_2				CaO
	Cubic phase		Tetragonal phase		Cubic phase
	Content, %	CSR, nm	Content, %	CSR, nm	Content, %
$S200_{Vac}$	93.26	51(2)	6.74	~ 6	0
$S400_{Vac}$*	94.46	56(3)	4.92	~ 9	0.62
$S900_{Vac}$**	89.50	$\gg 200$	6.50	~ 7	4.00
$S200_{Ar}$	94.50	49(2)	5.50	~ 7	0
$S400_{Ar}$*	94.19	50(3)	5.11	~ 6	0.70
$S900_{Ar}$	94.21	4.91	5	~ 7	0.88

* Samples with traces of CaO ($\sim$ 1%).
** Sample with traces of CaO ¿3%.

Ar correspond to the sample annealed in air, vacuum, and argon.

The following diagnostic techniques were applied in the examination of NP properties. A TriStar 3000 V6.03 analyzer was used to determine the texture properties of NPs by the Brunauer–Emmett–Teller (BET) method. X-ray diffraction (XRD) analysis was performed using a Discover D8 unit with a copper filter in accordance with standard procedures. Magnetic measurements were carried out with a Faraday balance at room temperature.

The variation of color of CaF_2 NPs under thermal annealing of color centers within the range from room temperature to 400°C was examined in [5]. It was demonstrated that a plum color of sample *S*0 changed to white after annealing at 400°C ($S400_{Atm}$), and the sample became almost equal in color intensity to the reference micrometer powder used to fabricate the target for evaporation. The same is true for samples *S*200 annealed in vacuum and argon. The results of texture analysis of CaF_2 NPs annealed in different media are listed in Table 1. All powders (except for *S*900) are mesoporous, which is evidenced by the hysteresis of type IV nitrogen adsorption/desorption isotherms. The hysteresis loop area depends on the annealing medium: the smallest and largest loops correspond to samples annealed in vacuum and argon, respectively. This is probably attributable to the fact that pores lose capillary condensate in the process of annealing in vacuum; in addition, the adsorption film on pore walls becomes thinner.

It can be seen from Table 1 that the SSA values of all samples tend to decrease with increasing annealing temperature. The samples annealed in air have the highest SSA, which is indicative of the fact that oxidation processes have a significant role in annealing. The SSA of samples annealed in vacuum and argon varies faster than the surface area of samples annealed in air. This may be attributed to their vacuum degassing in the furnace prior to annealing. However, the lowest SSA (with mesoporosity being retained) was exhibited by sample $S400_{Ar}$ annealed at 400°C. This is unexpected, since this sample had the maximum pore volume. The interparticle pore volume of samples first increased significantly as the annealing temperature rose to 400°C (the most noticeable variations correspond to annealing in air at 200°C and in argon at 400°C, where the volume increased by a factor of ~ 2.6 and ~ 1.7, respectively), but dropped sharply (by two orders of magnitude) after annealing at 900°C (Table 1).

The XRD analysis indicated the presence of three crystalline phases in CaF_2 samples: cubic and tetragonal CaF_2 fluorite phases and the cubic CaO phase (Table 2). The XRD data for samples *S*0, *S*200, and *S*900 annealed in air revealed only the fluorite phase, while the presence of CaO was determined based on the results of DSC-TG analysis [4].

The CaO content of samples increased with annealing temperature due to the oxidation of metallic Ca nanoparticles, which formed in CaF_2 NPs at the stage of synthesis and

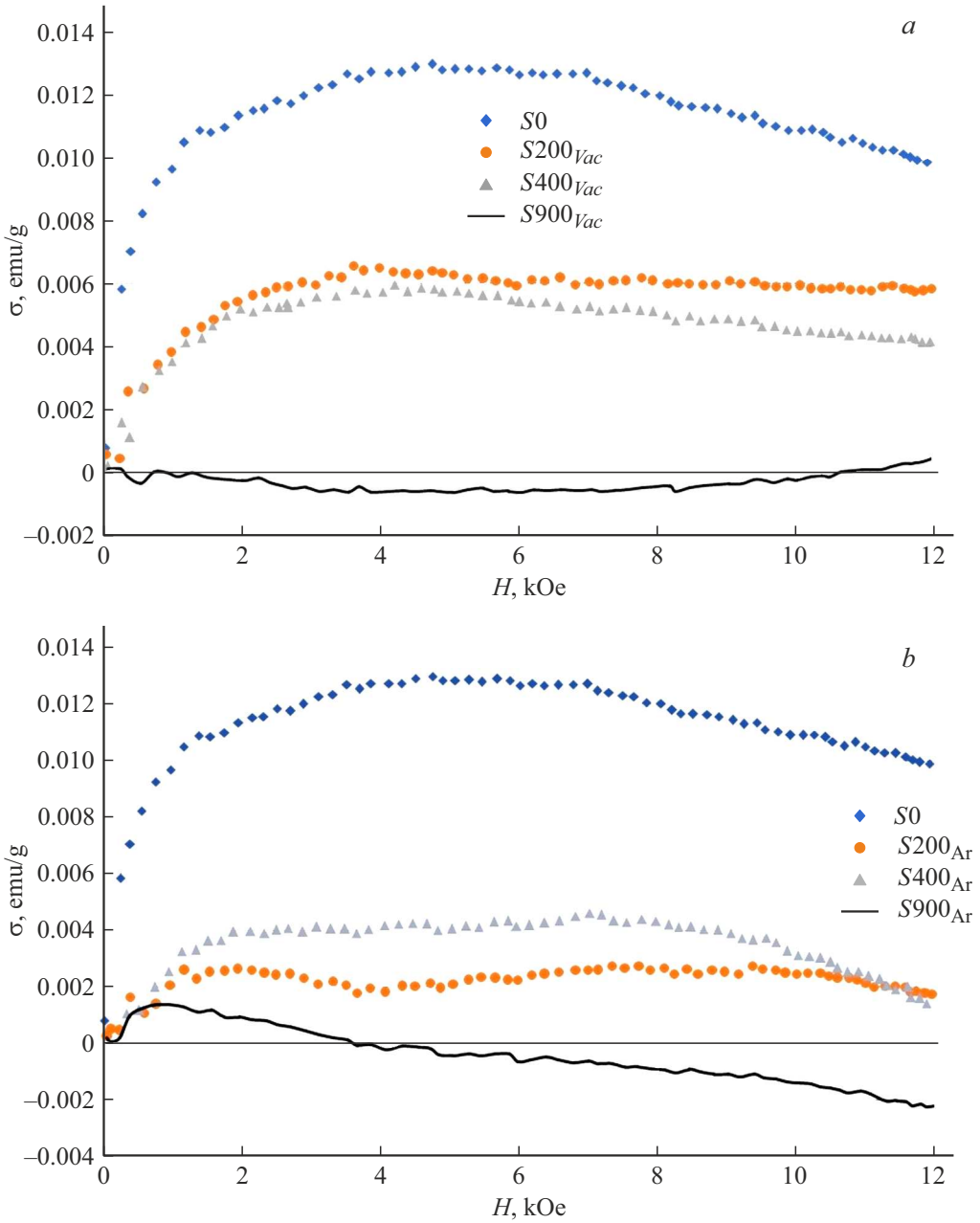

Specific magnetization curves of CaF_2 NPs annealed in vacuum (*a*), argon (*b*), and air (*c*).

adsorption of water vapor and CO_2 from the surrounding atmosphere during storage of nanofluoride.

The results of examination of the magnetic properties of NPs are presented in the figure. It can be seen that the magnetization of CaF_2 NPs changed after annealing, and the temperature and medium of preliminary NP annealing were of great importance in this case.

It follows from the figure (and the data reported earlier in [5]) that annealing in air leads to a considerable increase in magnetization of samples $S200_{Atm}$ and $S400_{Atm}$. Note that different batches of NPs have significantly discrepant absolute values of specific magnetization; for example, the data for sample *S*0 differ by a factor as high as 3 (0.044 and 0.012 emu/g in our study and in [4]). This is attributable to the instability of factors affecting the process of PEBE NP synthesis. However, the general variation trends remain the same. The retention of a substantial magnetization in sample $S900_{Atm}$ is especially intriguing in view of the fact that the micrometer powder, which was used to fabricate targets, has zero magnetization.

Annealing in vacuum leads to a sharp (twofold) reduction in magnetization of samples $S200_{Vac}$ and $S400_{Vac}$, while the magnetization of sample $S900_{Vac}$ vanished completely. A similar pattern was observed for samples annealed in argon, although certain quantitative differences were evident: the magnetization of samples $S200_{Ar}$ and $S400_{Ar}$ decreased by

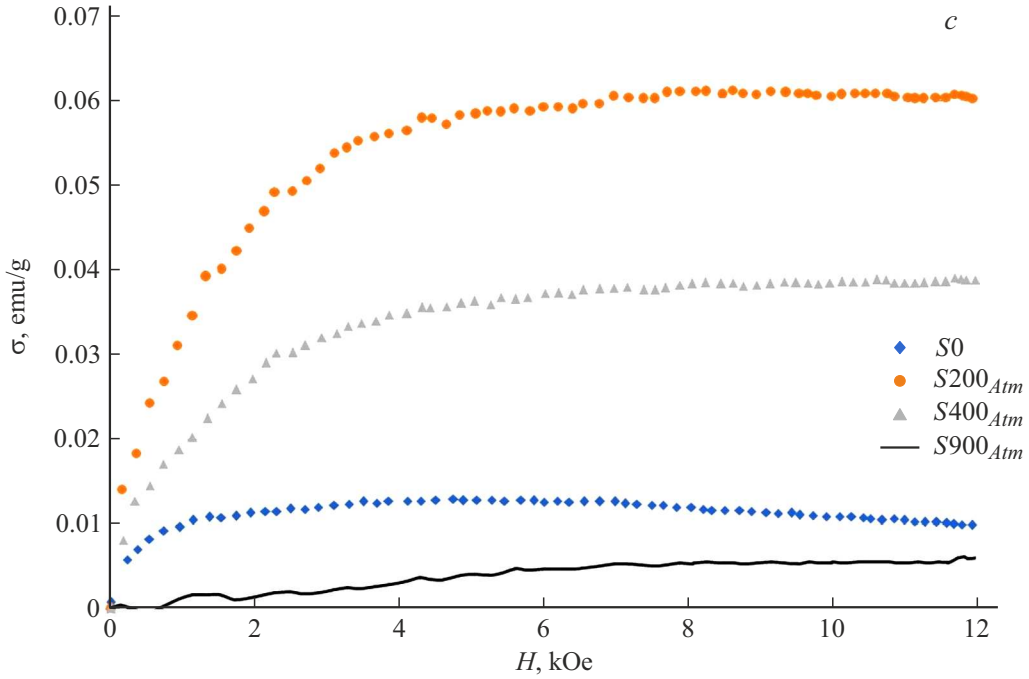

Figure (continued).

a factor of 6 and 3, respectively, and the magnetization of sample $S900_{Ar}$ vanished only in the region of magnetic fields > 4 kOe.

Therefore, the emergence of RTFM in CaF_2 NPs may be attributed to the formation of structural and radiation defects in the process of NP synthesis. Calcium and fluorine ions in bulk CaF_2 crystals do not feature a magnetic moment, since their electron shells are filled [5]. Annealing in air enhances RTFM, while annealing in air-free media suppresses it.

It is probable that the mechanism of oxidation of metallic calcium clusters and the formation of oxide CaO shells on the surface of fluoride nanoparticles, which proceeds most efficiently in the course of annealing of nanoparticles in air, are the governing factors here.

Thus, the influence of the annealing medium on texture, phase, and magnetic properties of CaF_2 NPs synthesized by PEBE has been observed for the first time.

Acknowledgments

The authors wish to thank I.A. Larin (Ural Federal University) for his help in experiments and T.M. Demina (Institute of Electrophysics, Ural Branch, Russian Academy of Sciences) for texture studies.

Funding

This study was supported in part by the Russian Science Foundation (project No. 22-19-00239).

Conflict of interest

The authors declare that they have no conflict of interest.

References

[1] V.V. Osipov, V.V. Lisenkov, V.V. Platonov, E.V. Tikhonov, Quantum Electron., **48** (3), 235 (2018). DOI: 10.1070/QEL16590.
[2] R.N. Grass, W.J. Stark, Chem. Commun, N 13, 1767 (2005). DOI: 10.1039/B419099H
[3] R.M. Rakhmatullin, V.V. Semashko, A.V. Lovchev, A.A. Rodionov, I.F. Gilmutdinov, A.G. Kiiamov, J. Magn. Magn. Mater., **541**, 168538 (2022). DOI: 10.1016/j.jmmm.2021.168538
[4] S.Yu. Sokovnin, V.G. Il'ves, M.E. Balezin, M.A. Uimin, Tech. Phys. Lett., **46** (4), 400 (2020). DOI: 10.1134/S1063785020040288.
[5] V.G. Il'ves, S.Yu. Sokovnin, M.G. Zuev, M.A. Uimin, M. Rähn, J. Kozlova, V. Sammelselg, Phys. Solid State, **61** (11), 2200 (2019). DOI: 10.1134/S1063783419110179.